# The ARH adaptor protein regulates endocytosis of the ROMK potassium secretory channel in mouse kidney

Liang Fang,[1] Rita Garuti,[2] Bo-Young Kim,[1] James B. Wade,[1] and Paul A. Welling[1]

[1]Department of Physiology, University of Maryland School of Medicine, Baltimore, Maryland, USA. [2]Department of Molecular Genetics, University of Texas Southwestern Medical Center, Dallas, Texas, USA.

**Renal outer medullary potassium (ROMK) channels are exquisitely regulated to adjust renal potassium excretion and maintain potassium balance. Clathrin-dependent endocytosis plays a critical role, limiting urinary potassium loss in potassium deficiency. In renal disease, aberrant ROMK endocytosis may contribute to potassium retention and hyperkalemia. Previous work has indicated that ROMK endocytosis is stimulated by with-no-lysine (WNK) kinases, but the endocytotic signal and the internalization machinery have not been defined. Here, we found that ROMK bound directly to the clathrin adaptor molecule autosomal recessive hypercholesterolemia (ARH), and this interaction was mediated by what we believe to be a novel variant of the canonical "NPXY" endocytotic signal, YxNPxFV. ARH recruits ROMK to clathrin-coated pits for constitutive and WNK1-stimuated endocytosis, and ARH knockdown decreased basal rates of ROMK endocytosis, in a heterologous expression system, COS-7 cells. We found that ARH was predominantly expressed in the distal nephron where it coimmunoprecipitated and colocalized with ROMK. In mice, the abundance of kidney ARH protein was modulated by dietary potassium and inversely correlated with changes in ROMK. Furthermore, ARH-knockout mice exhibited an altered ROMK response to potassium intake. These data suggest that ARH marks ROMK for clathrin-dependent endocytosis, in concert with the demands of potassium homeostasis.**

## Introduction

The renal outer medullary potassium (ROMK) (Kir1.1) subfamily of inward-rectifying potassium channels (1) plays an important role in potassium balance (2). Expressed on the apical membrane of distal nephron principal cells (3–5), these channels provide a final route for renal potassium secretion. They are regulated in accord with the demands of potassium homeostasis by plasma potassium, aldosterone, and other factors (6), ensuring potassium excretion precisely matches dietary intake. Because ROMK channels are constitutively open (1), regulated changes in channel function are largely brought about by alterations in the density of functional channels at the apical surface. In principle, this could occur by switching the channel activity on and off, by regulated recruitment and retrieval mechanisms, or by a combination of the 2 processes. In recent years, there has been increasing appreciation that membrane trafficking processes underpin ROMK regulation.

Clathrin-dependent endocytosis plays a central role (7). In states of dietary potassium deficiency, for example, ROMK channels are retrieved from the apical surface to limit urinary potassium loss and maintain potassium balance. By contrast, exaggerated ROMK endocytosis, in the face of normal dietary potassium intake, can lead to life-threatening hyperkalemia in renal disease. For example, in pseudohypoaldosteronism type II, a familial disorder of diminished renal potassium excretion and hypertension, alterations in with-no-lysine (WNK) kinases (8) have been reported to aberrantly stimulate ROMK endocytosis (9–11).

Despite its importance to physiology and disease, the molecular mechanisms responsible for ROMK endocytosis are still not well defined. A trafficking scaffold, intersectin, is believed to recruit the WNK kinases to clathrin-coated pits (12), but it is unknown how ROMK channels are similarly targeted to sites of endocytic retrieval. A potential clue comes from the discovery that mutations in a cytoplasmic C-terminal asparagine, $N_{375}$, dramatically increase ROMK cell surface expression (7) and render the channel resistant to WNK kinases (9, 10). Significantly, $N_{375}$ and the 3 neighboring residues form the sequence "NPXF," reminiscent of classic "NPXY" internalization signals in the LDL receptor and other members of the LDL receptor superfamily (13, 14). Although each of the residues in the NPXY signals are highly conserved in LDL receptors (15), the observations with ROMK raise the intriguing possibility that the channel uses an unusual variant of this canonical internalization signal.

The endocytotic sorting machinery that targets ROMK for internalization has also been a mystery. A preponderance of evidence indicates the conventional endocytotic clathrin adaptor, AP-2, does not directly interact with NPXY signals (15). Instead, a new and emerging class of clathrin-associated sorting proteins (CLASPs; ref. 16), featuring clathrin-interaction and AP-2–binding sequences and a phosphotyrosine-binding domain (PTB domain), has recently been implicated. Unlike that in typical PTB proteins, which act as cell signaling scaffolds and bind to a phosphotyrosine-containing motif (NPXYp), the PTB domain in the endocytotic adaptor proteins prefers binding to substrates that do not have a phosphorylated tyrosine (17), allowing the PTB-CLASPs to serve as recognition proteins for NPXY endocytosis signals. The 4 known PTB-CLASPs (disabled homolog 2 [Dab-2] [refs. 18–21]; Numb [ref. 22]; GULP/Ced-6 [ref. 23]; and autosomal recessive hypercholesterolemia [ARH] [refs. 24, 25], the product of the *ARH* gene [ref. 26]), have largely been studied in endocytosis of LDL receptor family members. Beyond the reported roles of Dab-2 and ARH in the endocytosis of a LDL receptor family member, megalin (20, 27), very little is known about the function of PTB CLASPs in

**Conflict of interest:** The authors have declared that no conflict of interest exists.
**Citation for this article:** *J. Clin. Invest.* **119**:3278–3289 (2009). doi:10.1172/JCI37950.

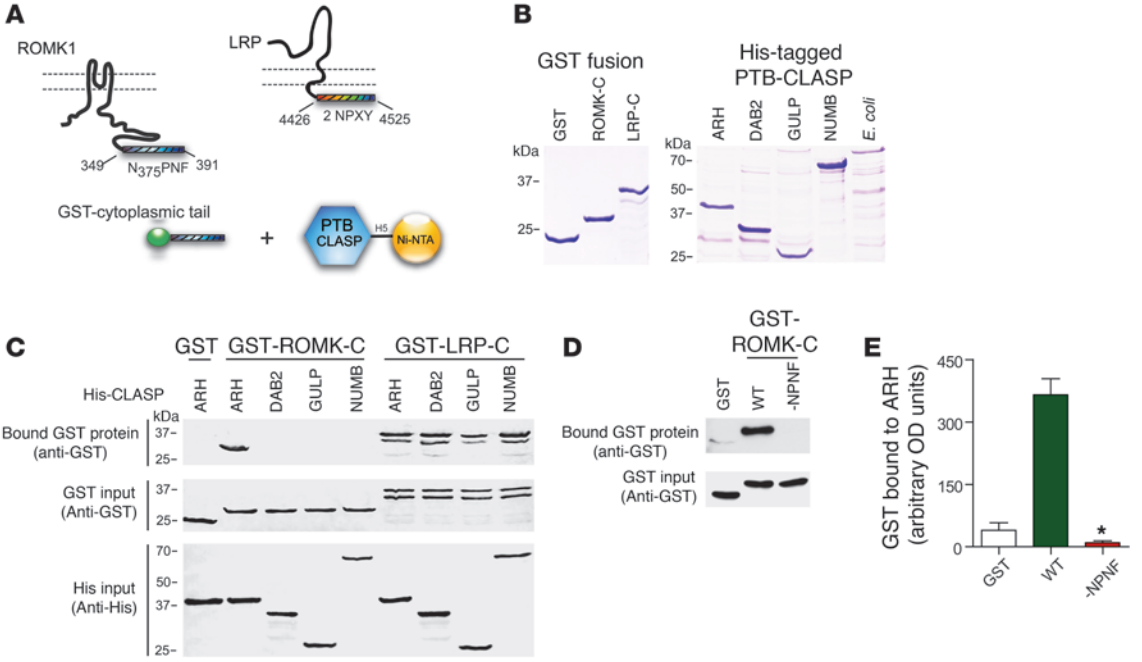


**Figure 1**

ROMK preferentially interacts with ARH. (**A**) Illustration of the pull-down assay. Recombinant His-tagged PTB-CLASPs (ARH, Dab2, Gulp, and Numb) were bound to Ni-NTA beads and tested for interaction with GST fusion proteins of either the ROMK C terminus or the LRP C terminus. H5, His-tag. (**B**) GST fusions of the WT ROMK1 C terminus (ROMK-C) (amino acids 349–391), LRP C terminus (LRP-C), and His-tagged PTB proteins were purified to homogeneity for the binding assay. Shown are purified proteins from *E. coli*–expressing indicated GST protein or His-tag CLASP, which had been resolved by SDS-PAGE and visualized by Coomassie Brilliant Blue staining and compared with vector-only–transfected *E. coli* (*E. coli*, BL21). (**C**) Binding assay. After incubation of GST proteins with each of indicated PTB-CLASPs, specifically bound protein (GST alone, GST ROMK C terminus [GST-ROMK-C], and GST LRP C terminus [GST-LRP-C] proteins) was assessed by immunoblot with anti-GST antibodies and compared with input GST (middle row) and HIS-tagged proteins (bottom row). GST-ROMK-C preferentially bound to ARH, while GST-LRP-C bound all the PTB-CLASPs. As observed before (23), GST-LRP-C migrates as doublet due to partial proteolysis. (**D** and **E**) ARH interacts with ROMK in an NPXF signal–dependent manner. Binding of ARH with GST, GST-ROMK-C, and a mutant GST-ROMK-C, bearing an alanine replacement of the $N_{375}$PNF sequence (-NPNF). (**E**) Quantification of binding. $n = 3$; $^*P < 0.001$.

the kidney. Here, we test whether they recognize a unique internalization signal in ROMK and target the channel for endocytosis.

## Results

*Identification of ARH as a ROMK-binding partner in the kidney*. To explore the involvement of PTB-domain containing clathrin-adaptor molecules in ROMK endocytosis, we screened each of them (ARH, Dab-2, GULP, and Numb) for ROMK binding capacity (Figure 1A). A glutathione-*S*-transferase (GST) fusion protein of the extreme C terminus of ROMK (amino acids 349–391), containing the "NPNF" motif, was constructed, purified to homogeneity, and combined with purified His-tagged PTB-CLASPs immobilized on Ni-NTA beads (Figure 1B). The C-terminal tail of the LDL receptor–related protein (LRP) was also produced as a GST fusion and used as a positive control for CLASP interaction, because it contains 2 functional NPXY motifs (23). After extensive washing, material specifically bound to ARH, Dab2, GULP, or Numb was eluted and detected in Western blot with anti-GST antibodies. In contrast to LRP, which bound to all the PTB-CLASPs, ROMK preferentially bound to ARH. Importantly, alanine replacement (AAAA) of the NPNF tract in ROMK completely abrogated ARH binding (Figure 1, D and E), consistent with a highly specific endocytotic signal recognition interaction.

To test the physiological relevance of the interaction, we examined ARH and ROMK in the native kidney. As observed by immunofluorescence and confocal microscopy, ARH colocalized with ROMK in subapical and perinuclear compartments in the distal nephron principal cells (Figure 2, A–C). In fact, ARH predominantly localizes to nephron segments involved in controlling potassium balance and in the distal nephron (DCT, CNT, CCD) and to a minor extent in the thick ascending limbs (TALs) (Figure 2D), distinct from the preponderate localization of Dab-2 in the proximal tubule (20).

ROMK also coimmunoprecipitates with ARH from kidney extracts on anti-ARH antibody-bound beads but not with an unrelated IgG (Figure 2E), indicating ARH specifically interacts with ROMK in vivo. Similar studies with different antibodies and HA epitope–tagged ROMK and myc-tagged ARH in COS-7 cells further corroborate the specificity of the ARH-ROMK coimmunoprecipitation (Figure 2, F and G). Importantly, alanine replacement of the NPNF motif in ROMK completely abrogated the ARH-ROMK coimmunoprecipitation, supporting the requirement of the amino acid track for the interaction.

*ARH facilitates ROMK endocytosis*. The ability of ARH to interact with ROMK in an NPNF-dependent manner suggests a capacity to function as an endocytic adaptor. To test whether ARH actually stimulates ROMK endocytosis, surface biotinylation studies were performed in COS-7 cells. In these studies, external flag epitope-tagged ROMK channels at the plasmalemma were specifically labeled with a cell-impermeant form of biotin (sulfo-NHS-SS-bio-

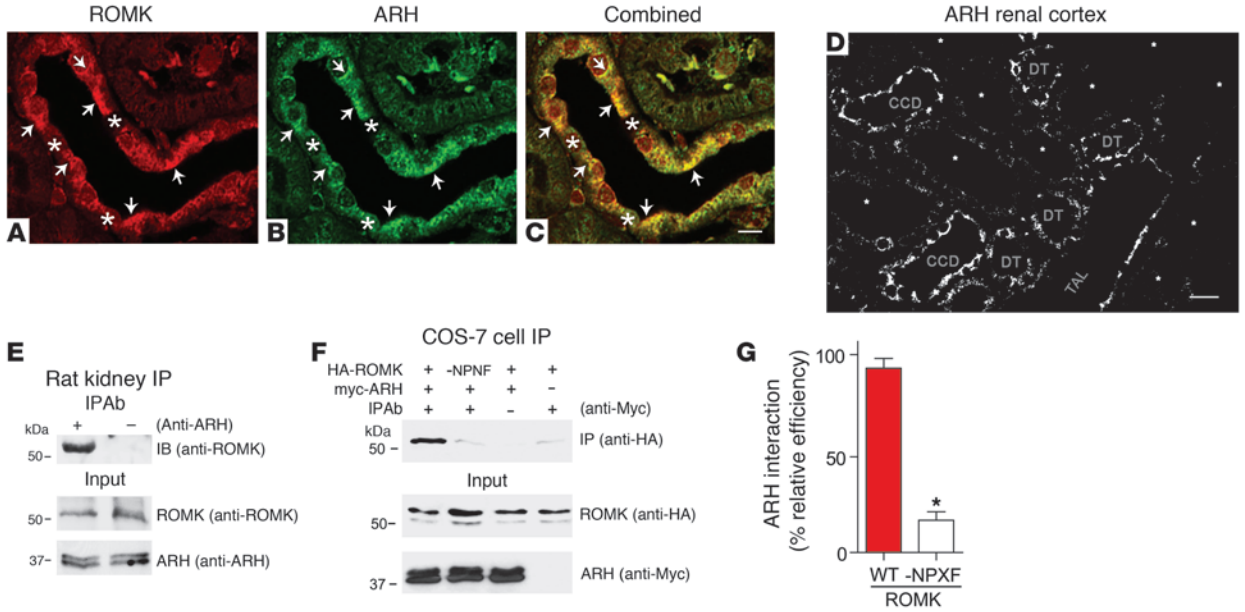


**Figure 2**

Colocalization and coimmunoprecipitation of ARH and ROMK in the rat kidney. Immunofluorescent staining of (**A**) ROMK with a chicken anti-ROMK antibody and (**B**) ARH with a goat anti-ARH antibody (**C**) and colocalization of ARH (green) and ROMK (red) in a rat kidney collecting duct, using appropriate, specific Alexa Fluor–conjugated secondary antibodies. Arrowheads indicate subapical or perinuclear labeling in principal cells; asterisks indicate intercalated cells. Scale bar: 8.5 μm. (**D**) Low-power confocal microscope image of ARH localization in cortex of rat kidney. ARH can be detected in cortical collecting ducts (CCDs), TALs, and distal tubules (DTs), but little or no labeling is detected in proximal tubules (asterisks). Collecting ducts were identified based on double labeling with antibody to AQP2 raised in chicken and other segments identified based on morphological criteria. Scale bar: 8 μm. (**E**) Immunoprecipitation analysis of ROMK channel with ARH from whole rat kidney extracts. (**F**) Immunoprecipitation of HA epitope–tagged ROMK or mutant ROMK, lacking the NPNF motif, with myc-tagged ARH from COS-7 cells transfected with indicated (+) cDNAs. Only WT ROMK was immunoprecipitated with ARH. (**G**) Quantification of IP results. $n = 3$; $^*P < 0.001$.

tin), recovered on neutravidin beads, and then detected in Western blot with anti-ROMK antibodies. Coexpression of ARH led to a dramatic, time-dependent attenuation of ROMK cell surface expression (Figure 3, A and B) In principle, the response may be due to altered biosynthetic delivery, exocytosis, recycling, postendocytotic trafficking to nonrecycling compartments, degradation, or a combination of these processes. To test whether the inhibitory effect of ARH involves augmented endocytosis, internalization rates were measured directly. In these studies, cell surface channels were first labeled with sulfo-NHS-SS-biotin (4°C, as above) and then returned to 37°C to initiate endocytosis. After variable amounts of time, cells were returned to 4°C and the biotin molecules that remained at the cell surface were stripped with an impermeable reducing agent, MesNa. Internalized channel proteins remain biotinylated after MesNa treatment and therefore can be recovered on neutravidin beads and detected in Western blots with anti-ROMK antibodies. As shown in a representative experiment (Figure 3C), increasing amounts of biotinylated channel became resistant to MesNa cleavage over the rapid time course. Considerably more internalized channel was detected over the entire chase period in cells expressing ARH compared with cells transfected with empty vector (Figure 3D). In fact, as measured in the most linear portion of the time course (0–5 minutes), ARH expression led to a dramatic and statistically significant attenuation of the internalization rate (Figure 3E). Taken together, these data demonstrate that ARH stimulates ROMK internalization.

*ARH drives ROMK endocytosis in an NPNF-dependent manner*. To determine whether the NPNF motif is required for ARH-dependent ROMK endocytosis, we performed domain transplantation studies with Kir2.1, a close relative of ROMK (shares ~60% amino acid identity), which does not contain NPXY or NPXF motifs (Figure 4). As measured by cell surface HA-antibody binding, ARH had no effect on the expression of external HA epitope–tagged Kir2.1 at the plasmalemma (Figure 4B). By contrast, channels acquired sensitivity to ARH when the Kir2.1 C terminus was replaced with the comparable ROMK domain, containing the NPNF sequence. Indeed, coexpression of ARH with the Kir2.1/ROMK chimera (N2.1/ROMK chimera) caused a dramatic attenuation of channel surface expression (Figure 4B). Replacement of the $N_{375}$PNF tract in the N2.1/ROMK chimera with 4 alanines increased surface expression and rendered the channel resistant to ARH. Thus, the NPNF motif in ROMK is necessary and sufficient for ARH action. In agreement with preferential binding of ARH to ROMK, the reduction in channel surface expression was only observed with ARH and not the other PTB-CLASPs (Figure 4C).

To test whether the suppressive effects of ARH on N2.1/ROMK surface expression were actually due to stimulation of endocytosis, we directly measured channel internalization using an "antibody feeding" assay (Figure 5). In these studies, live COS-7 cells, expressing external HA epitope–tagged N2.1/ROMK channels, were incubated with anti-HA antibody in the cold to label the channels at the cell surface and then shifted to 37°C to initiate internalization. Following different incubation times at 37°C, the anti-HA labeled channels that remained on the surface were detected with saturating amounts of an Alexa 488–conjugated (green) secondary antibody. Internalized channels, which were labeled at the cell surface

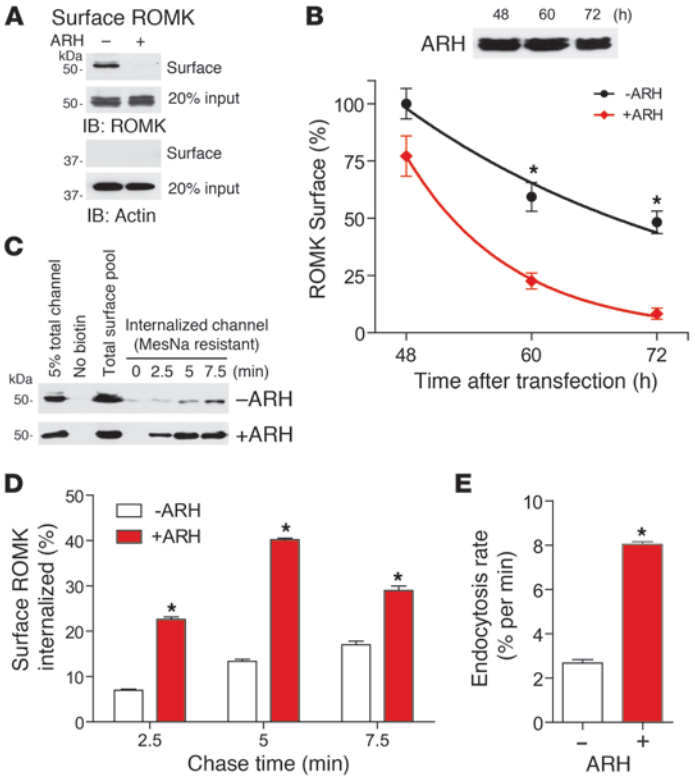


**Figure 3**
ARH promotes ROMK endocytosis. (**A**) COS cells were cotransfected with ROMK and ARH (+ARH) or empty vector (–ARH). Shown are typical results of surface ROMK, as detected in Western blot with ROMK antibodies, following cell surface biotinylation and neutravidin recovery, 72 hours after transfection. Surface is compared with total cell input of ROMK. Actin is not labeled by biotin, confirming biotinylation is specific for surface proteins. (**B**) Quantification of channel cell surface expression in the absence (black circles) and presence of exogenous ARH (red squares) at posttransfection times indicated ($n = 3$). ROMK surface expression is normalized to the average at time 0. The inset shows a Western blot of ARH in ARH-transfected cells over the time course. *$P < 0.01$. (**C**) Direct measurements of ROMK endocytosis in COS cells in the absence and presence of ARH (48 hours after transfection). Surface channels were labeled with sulfo-NHS-SS-biotin in the cold and then incubated at 37°C to permit endocytosis for variable times (0–7.5 minutes). Biotin remaining at the cell surface was cleaved with the reducing agent, MesNa, and internalized (biotinylated) proteins were recovered with neutravidin-conjugated beads and detected along with the total surface pool in immunoblots, using an anti-ROMK antibody. No proteins were captured on neutravidin beads without prior biotinylation (second lane). (**D**) Quantification of internalized channel relative to the surface pool at each time point by densitometry (mean ± SEM; $n = 3$). *$P < 0.01$. (**E**) Rates of ROMK endocytosis in the absence and presence of exogenous ARH. *$P < 0.01$.

with the anti-HA antibody, were detected with a different secondary antibody, Alexa 568 (red), following cell permeabilization (see Figure 5A for experimental scheme). As shown in Figure 5B and quantified in Figure 5C, coexpression of ARH led to a dramatic increase in internalization of N2.1/ROMK channels. Replacement of $N_{375}$PNF with 4 alanine residues completely inhibited the response. Taken together, these data provide direct evidence that ARH stimulates ROMK endocytosis in an NPNF-dependent manner.

*The internalization signal in ROMK is an ARH recognition site.* If ARH directly interacts with ROMK to mark channels for endocytosis, the sequence of the internalization signal should be identical to the sequence that is recognized by ARH. To test this, we first sought to determine the precise sequence of the endocytosis signal. Strong NPXY signals conform to a hexapeptide motif, [FY]xNPXY (28), and initial alanine-cassette mutagenesis studies revealed residues neighboring the $N_{375}$PNF tract are necessary for ROMK endocytosis (data not shown). Consequently, we tested the requirements of each residue in the $N_{375}$PNF tract as well as 2 flanking amino acids in channel endocytosis. Individual residues were replaced with alanine, and mutant channels were screened for ARH-dependent endocytosis by measuring cell surface expression in the absence and presence of exogenous ARH. Mutations were first tested in the external HA epitope–tagged N2.1/ROMK chimera, because robust cell surface expression of this construct permits quantitative antibody binding measurements at the cell surface in a large number of parallel samples (Figure 6A). Western blot analysis verified that the mutant channels were equally expressed and cells contained equivalent levels of ARH (data not shown). Of the 8 mutants tested, 5 (Y373A, N375A, P376A, F378A, and V379A) increased cell surface expression and caused channels to become resistant to ARH (Figure 6A), as predicted for the specific disruption of an ARH-dependent internalization signal. Formal measurements of endocytosis in the ROMK channel by surface biotinylation revealed that each of the mutations suppressed endocytosis (Figure 6B). Thus, the ARH-dependent internalization signal in ROMK is defined by a sequence that we believe to be novel, YxNPxFV.

To test whether the sequence requirements for ARH interaction are the same as those for the endocytotic signal, alanine-replacement mutations were introduced into the residues of the relevant region as described above, and direct ARH binding was assessed in the recombinant protein-protein interaction assay. As shown in Figure 6C and quantified in Figure 6D, mutations at Y373, N375, P376, F378, and V379 (but not D373, N377, and L380) dramatically attenuated binding to ARH. The consequential residues precisely correspond to the endocytosis signal as mapped above. Taken together, these data indicate the internalization signal acts as a recognition site for ARH interaction.

*ARH couples YxNPxFV signal recognition to clathrin coated-pit localization.* The modular nature of ARH (Figure 7A) provides a scaffolding architecture to couple cargo selection to clathrin-pit localization (25, 29). If the internalization signal in ROMK associates with ARH in a manner like canonical NPXY signals, direct interaction with the PTB domain would free the C-terminal domains in ARH for clathrin nucleation and coated-pit targeting. To test this scaffolding mechanism, we examined the consequence of removing the clathrin and AP-2–binding domains from ARH (Figure 7A). As measured by immunoprecipitation (Figure 7B), the WT ARH associated with ROMK, AP-2, and clathrin. By contrast, the C-terminal ARH truncation mutant ($ARH_{1–187}$), lacking the clathrin and AP-2–binding domains, was able to support interaction with ROMK but not with clathrin or AP-2α (Figure 7B). Thus, ROMK interacted with the PTB-domain as predicted. Direct measure-

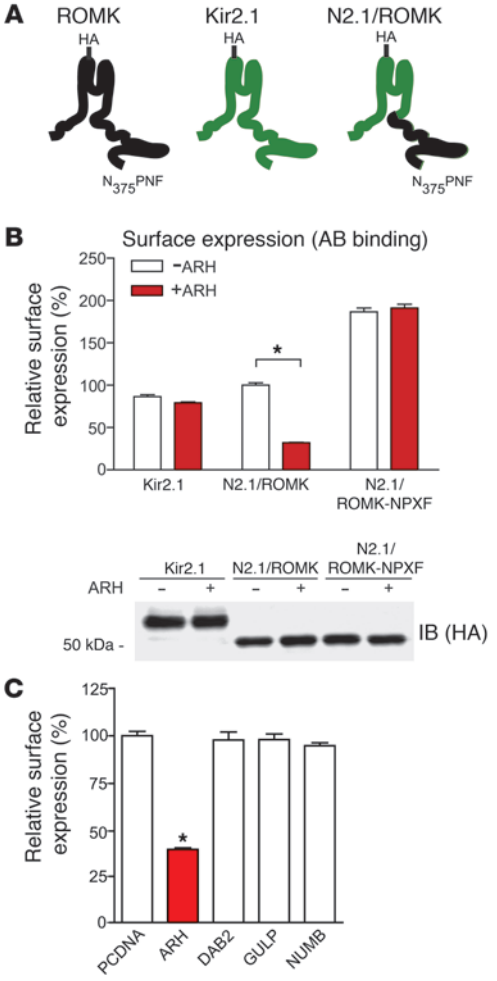


**Figure 4**

ARH specifically reduces ROMK surface expression in a signal-dependent manner. Evidence from domain transplantation. (**A**) Cartoon of external HA-tagged ROMK, Kir2.1, and the N2.1/ROMK chimera. (**B**) Cell surface expression as measured by HA Ab binding and luminometry of indicated external HA-tagged channels (WT Kir2.1, N2.1/ROMK, and N2.1/ROMK mutant, in which the NPNF motif was replaced with AAAA) in COS cells in the absence (white bars) and presence of exogenous ARH (red bars). $n = 3$. In a representative blot, total cellular input of the different channel proteins, as detected in anti-HA immunoblots, is not influenced by ARH. (**C**) N2.1/ROMK cell surface expression as measured by HA Ab binding and luminometry in COS cells cotransfected with empty vector (PCDNA) or PTB-CLASPs indicated. $n = 3$; $^*P < 0.001$.

ments of ROMK endocytosis offered further evidence of a scaffolding mechanism (Figure 7, C and D); unlike the WT ARH, which enhanced ROMK endocytosis, the $ARH_{1–187}$ mutant was unable to drive channel internalization. In fact, because $ARH_{1–187}$ interacts with ROMK but not with clathrin or AP-2, it exerted a dominant-negative response, displacing the channel from endogenous ARH and blocking ROMK endocytosis. To corroborate this observation, we tested the role of endogenous ARH in basal ROMK endocytosis using ARH-specific siRNA in COS cells (Figure 7, E and F). ARH siRNA probes knocked down endogenous ARH but had no effect on a housekeeping marker, COX IV, consistent with a specific response. Compared with mock or nontargeting negative control siRNA-transfected cells, ROMK endocytosis was almost completely inhibited in cells depleted of ARH. Taken together, these observations indicate that ARH is required for basal ROMK endocytosis, recruiting the channels to clathrin-coated pits by simultaneously interacting with the internalization signal, clathrin, and AP-2.

*Long isoform of WNK1 stimulates ROMK endocytosis in an ARH-dependent fashion*. Present evidence indicates that the long isoform of WNK1, L-WNK1, physiologically limits renal potassium excretion (10, 11, 30) by suppressing ROMK surface expression. Because the response can be abrogated by dominant-negative dynamin or by a mutation in the ROMK $N_{375}$ residue, it has been supposed that L-WNK1 stimulates ROMK endocytosis (10, 12). To critically examine this idea and explore the involvement of ARH, we measured ROMK endocytosis directly following expression of the L-WNK1 active fragment and either WT ARH or dominant-negative ARH, $ARH_{1–187}$. As shown in Figure 8, expression of L-WNK1 nearly tripled ROMK internalization, revealing for the first time that L-WNK1 stimulates ROMK endocytosis. Importantly, the response was completely blocked by the dominant-negative form of ARH, $ARH_{1–187}$. Thus, ARH is required for WNK1-stimulated ROMK internalization.

*Role of ARH in the kidney*. Our discovery that ARH is required for basal and L-WNK1–stimulated endocytosis in cell expression systems, together with the identification of ARH as a ROMK-binding partner in the kidney, raise the possibility that ARH might participate in the physiological regulation of the channel. To test this, we first determined whether ARH protein levels in the kidney are modulated by dietary potassium, as a part of the homeostatic potassium balance response. Identical to observations in cell expression systems, the mouse kidney ARH protein migrated on SDS-PAGE gels as a doublet (Figure 9A); because alkaline phosphatase treatment collapses the doublet into a single band (data not shown), phosphorylation is likely responsible. As shown in the representative immunoblot (Figure 9A) and quantified in Figure 9B, both ARH bands were greater in kidneys of mice fed a low-potassium diet (4 days) compared with animals fed a high-potassium diet. The ARH response correlates inversely with reported changes in ROMK activity (31–33), just as would be predicted if ARH-dependent ROMK endocytosis is stimulated in states of potassium depletion and suppressed in states of potassium excess to regulate the channel abundance in accordance with the demands of potassium balance. To test the role of ARH on ROMK regulation, renal cortical ROMK protein was evaluated in ARH-knockout mice, which do not express ARH in the kidney (Figure 9B), and then compared with WT littermates fed different potassium diets. We confirmed that a low-potassium diet reduces ROMK protein abundance in WT animals, compared with a high-potassium diet, a response that primarily reflects a difference in the complex glycosylated ROMK protein. In contrast, a low-potassium diet did not alter ROMK abundance in ARH null mice. The effects of dietary potassium intake were significantly different ($P = 0.004$) between ARH null animals (13% ± 10% change in ROMK abundance) and WT animals (46.77% ± 6% change in ROMK abundance). Regardless of potassium intake, ROMK in the ARH null animals was as abundant as observed in WT animals fed the high-potassium diet. Taken together, these studies indicate that ARH plays an important role in physiologically regulating ROMK.

## Discussion

ROMK surface expression is controlled by clathrin-dependent endocytosis in the distal nephron, limiting potassium excretion in

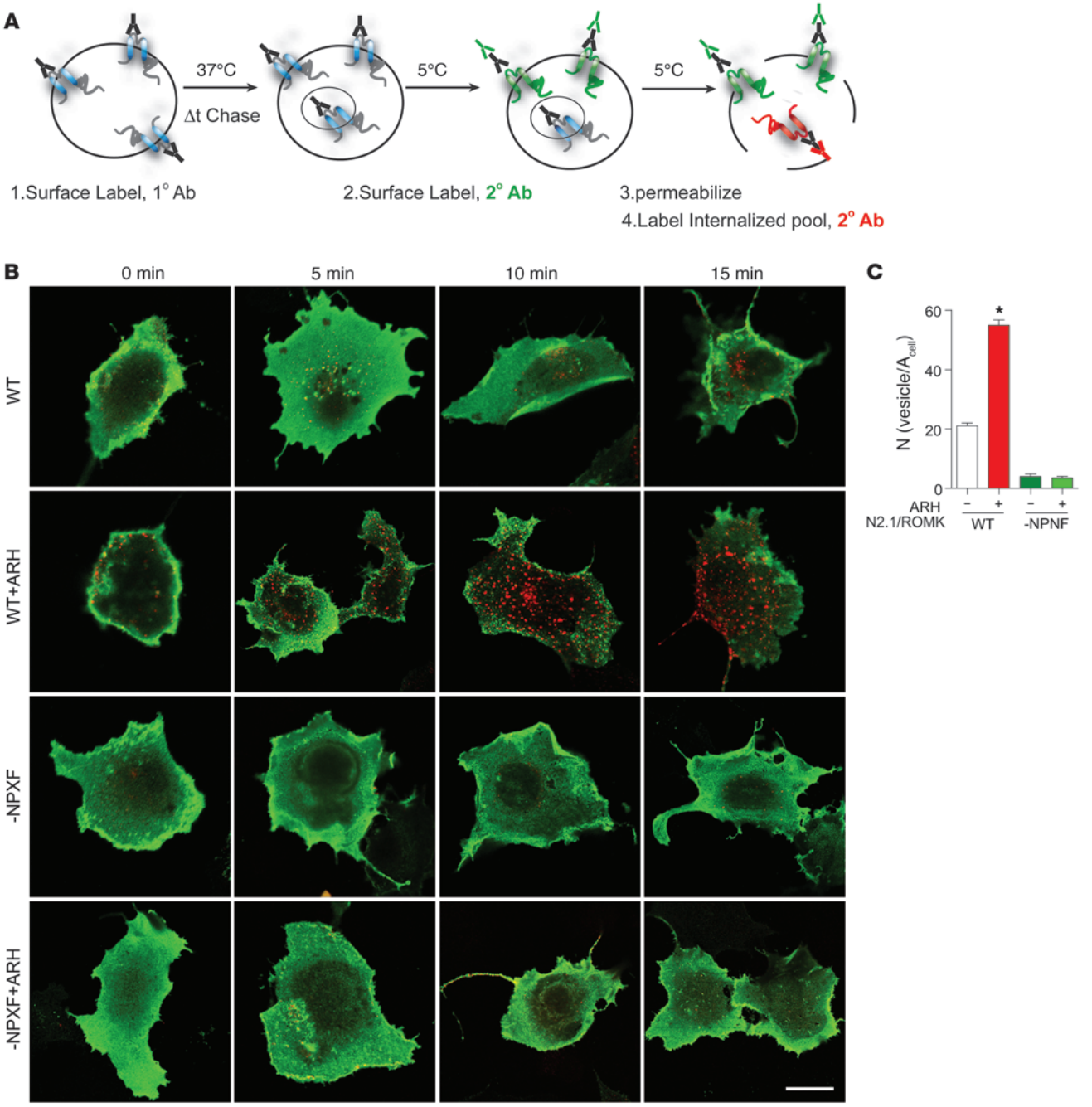


**Figure 5**

ARH stimulates channel endocytosis in a signal-dependent manner. Evidence from domain transplantation. (**A**) Cartoon of the antibody feeding endocytosis assay. (**B**) Typical cells transfected with the N2.1/ROMK chimera or the mutant, in which the NPNF motif was replaced with AAAA in the absence ARH (top panel) and presence of ARH (bottom panel) at indicated chase times after surface labeling. Green indicates the surface channel; red indicates the internalized channel. Note the increase in red puncta in the cells cotransfected with N2.1/ROMK and ARH. Scale bar: 10 μm (all panels have equivalent dimensions). (**C**) Quantification of endocytosis (N, vesicle number per unit cell area at the 15 minute chase time) for WT N2.1/ROMK chimera and NPNF mutant N2.1/ROMK, in the absence and presence of exogenous ARH. $n = 5$ cells for each condition (*$P < 0.001$).

states of potassium deficiency (34). Here, we elucidate the mechanism and identify what we believe to be a new component in the WNK1 signal transduction pathway. We found ROMK contains an unusual variant of the NPXY internalization motif. The signal serves as a specific recognition site for binding to ARH, a member of the PTB-domain containing clathrin adaptors. ARH stimulates ROMK endocytosis in a manner that is dependent on the internalization signal. Indeed, the sequence determinants of ARH-ROMK interaction precisely match the sequence requirements for ARH-dependent ROMK endocytosis. Because the ROMK signal binds to

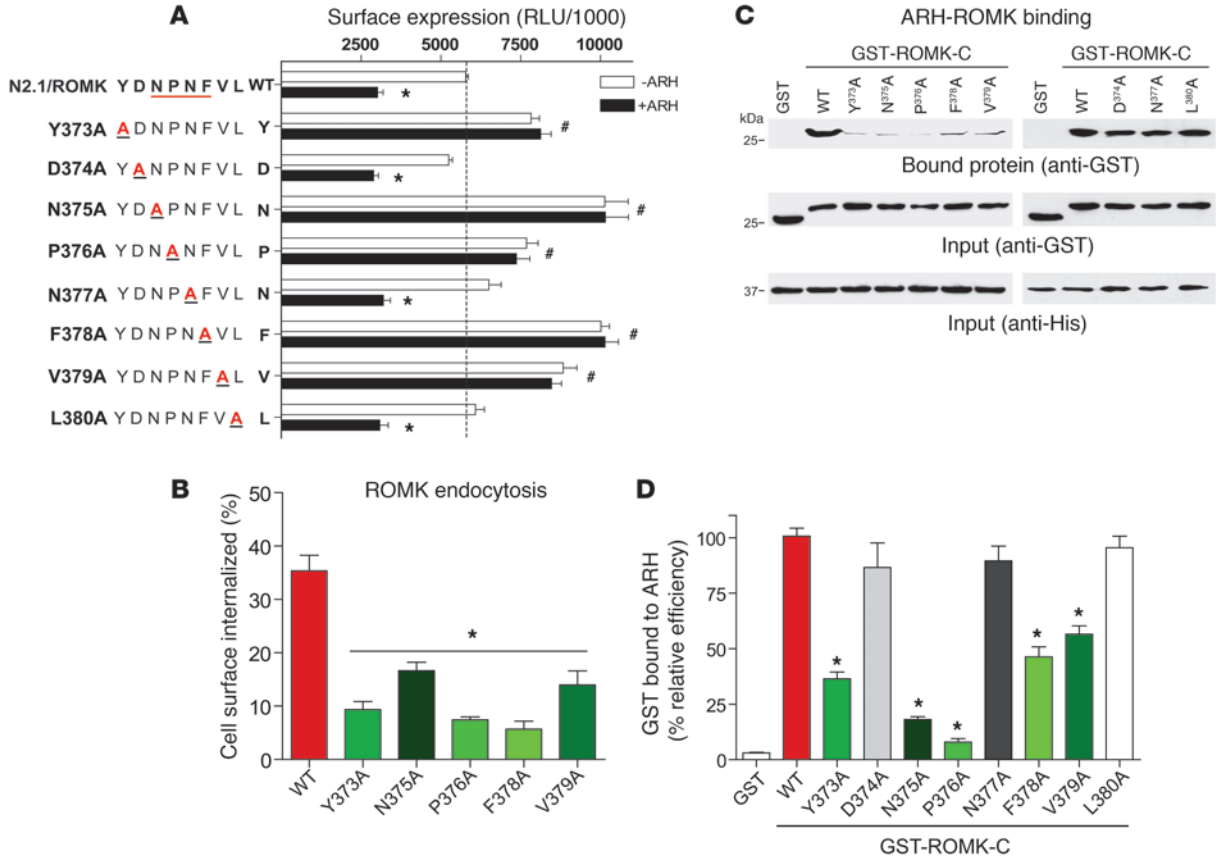


**Figure 6**

ROMK sequence requirements of ARH-dependent internalization match the requirements of ARH binding. (**A**) Mapping the sequence of the endocytotic signal. Point mutations each residue of the putative trafficking signal ($YDN_{375}PNFVL$) were created in the N2.1/ROMK channel and cell surface expression was measured by HA antibody binding and cell surface luminescence (RLU) in the absence (white bars) and presence of ARH (black bars). Comparison of individual constructs in the absence and presence of ARH showed that cell surface expression in the presence of ARH was significantly smaller than in absence of ARH (* $P < 0.001$). Comparison of the mutants versus WT channel showed that the mutants had significantly greater cell surface expression than WT channel (#$P < 0.05$; $n = 3$). Total cellular input of channel protein was not influenced by ARH (data not shown). (**B**) Endocytosis of ROMK (WT ROMK and indicated mutants) was measured with the biotinylation internalization assay (5 minute time point) in COS-7 cells expressing exogenous ARH. Y373A, N375A, P376A, F378A, and V379A mutants attenuated endocytosis. $n = 3$; *$P < 0.001$. (**C**) Representative GST-ROMK/His-ARH interaction assay with WT ROMK and indicated mutants. (**D**) Quantification of ARH interaction of GST, WT GST-ROMK-C, and mutant GST-ROMK-C. $n = 3$; *$P < 0.01$.

ARH via the PTB domain, ARH effectively marks ROMK channels for internalization by simultaneously engaging AP-2 and clathrin through different structures. ARH-dependent endocytosis provides a mechanism to regulate ROMK in accordance with the demands of potassium balance.

*Endocytosis signal is a preferential recognition site for ARH interaction*. Our identification of the YxNPxFV internalization motif in ROMK expands the spectrum of NPXY-type endocytotic signals. Although ROMK contains the "YxPN" core sequence of the archetypal internalization signal ($[Y/F]_{-3}xN_{-2}P_{-1}xY_0$, the key tyrosine defines the 0 position in the motif), the COOH-end exhibits 2 noteworthy differences. Certainly, replacement of the key tyrosine ($Y_0$) with phenylalanine represents a remarkable departure from the norm. First recognized from a LDL receptor mutation in a familial hypercholesterolemia patient (35), the tyrosine $Y_0$ is absolutely conserved in the entire LDL family of receptors (13). In fact, with the possible exception of the putative internalization signal in the CD18 subunit of the human complement receptor (36), $Y_0$ is found in all known NPXY signals (15). Mutant analysis of the canonical signal in LDL receptor proteins revealed that substitution of $Y_0$ with phenylalanine can variably reduce internalization efficacy (13, 28), depending on the receptor and the structural context of the signal. It is likely that strong internalization is maintained in ROMK, despite the natural $Y_0$ to F replacement, because the signal is extended by 1 residue, $V_{+1}$. Presumably, this provides an additional source of PTB energy as observed with the NAK peptide binding to the Numb PTB domain (37). Together, the 2 C-terminal deviations in the ROMK signal may also contribute to the tight binding specificity, explaining why ROMK preferentially interacts with ARH, while the canonical signal allows promiscuous binding to all known PTB-CLASPs.

*A function for ARH in kidney*. Our observations reveal a central function of ARH in the kidney and the regulation of potassium balance. First identified as the product of the *ARH* gene (26), ARH has been studied largely in the liver, in which it promotes LDL receptor endocytosis and plays a critical role in LDL clearance (18, 24,

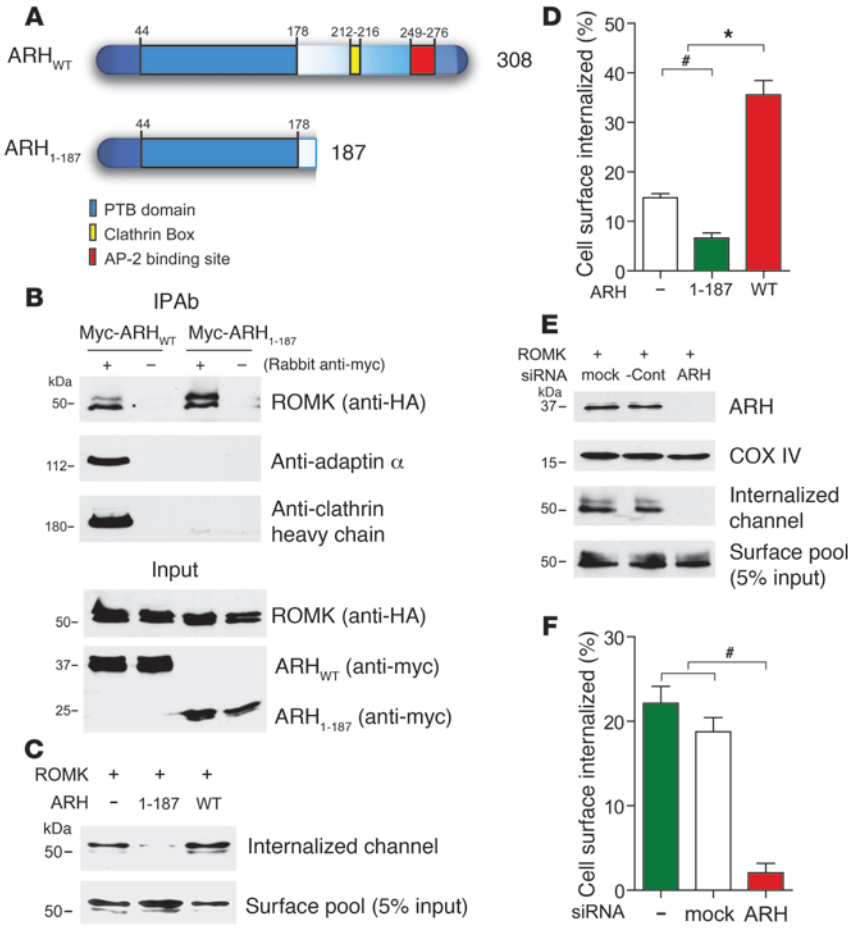


**Figure 7**
ARH couples YxNPxFV signal recognition to clathrin coated-pit localization. (**A**) Cartoon of the ARH domain structure. WT ARH is compared with $ARH_{1–187}$, a truncation mutant comprised of the PTB domain. (**B**) Interaction of ARH with ROMK, clathrin, and AP-2 was assessed by anti myc-immunoprecipitation. COS-7 cells were cotransfected with HA-tagged ROMK and either myc-tagged WT ARH (left columns) or $ARH_{1–187}$ (right columns). Myc-antibody (+) or mock antibody (-) immunoprecipitation was followed by immunoblotting for ROMK (HA antibody), clathrin (anti–heavy chain antibody), or AP-2 (α-adaptin antibody) and compared with input. (**C**) ROMK endocytosis measured by biotinylation in cells cotransfected with WT ARH, $ARH_{1–187}$, or empty vector (-). Surface biotin-labeled ROMK internalized after a 5-minute chase is compared with the total surface pool. (**D**) Quantification of ROMK endocytosis of groups above. ($n$ = 3; $^*P < 0.001$ greater than control; $^{\#}P < 0.05$ less than control.) (**E**) siRNA-mediated knockout of endogenous ARH blocks ROMK endocytosis in COS cells. ARH protein and ROMK endocytosis was measured in cells cotransfected with ROMK or no siRNA (MOCK), nontargeting siRNA (control [-cont]) or ARH-specific siRNA probes. The top 2 panels are representative immunoblots of ARH relative to a loading control (COX IV). The bottom 2 panels are surface-labeled ROMK internalized after a 5-minute chase compared with the total surface pool. (**F**) Quantification of ROMK endocytosis in groups above. $n$ = 3; $^{\#}P < 0.05$ less than both controls.

38–41). Yet, as noted with the discovery of ARH, robust ARH expression in the kidney (26) implied functions beyond lipid metabolism. One possibility was raised by observations in model systems that ARH promotes endocytosis of megalin (27), a proximal tubule LDL-like receptor that is responsible for protein reabsorption (42, 43). However, we found that ARH is not detectable in proximal convoluted tubules, in which megalin is most abundant. Compared with the low levels in TALs, ARH is strongly expressed at the major sites of regulated potassium secretion in the kidney (the distal convoluted tubule, connecting segment, and collecting duct). The predominant expression pattern of ARH in the distal nephron provides a mechanism to specifically regulate ROMK endocytosis in the distal nephron. Certainly, our finding that ARH is regulated by dietary potassium, together with the observation in ARH-knockout mice that ARH is required for appropriate regulation of ROMK protein abundance by dietary potassium, implies that ARH plays an important role in the potassium balance response of the kidney.

It will be important to carefully examine renal potassium handling in patients with autosomal recessive hypercholesterolemia. Given the preferential binding of ROMK for ARH over other PTB-CLASPs, predominate expression of ARH in the distal nephron, and our observations in *Arh*$^{-/-}$ mice, ARH appears to play a major role in ROMK endocytosis, reducing renal potassium excretion in states of dietary potassium deficiency. Our observations predict patients with autosomal recessive hypercholesterolemia, who lack ARH, may have difficultly reducing urinary potassium loss and thus, may exhibit altered potassium balance when provoked by dietary potassium depletion.

*ARH is a component of the WNK1 pathway.* Since the discovery that mutations in the WNK1 and WNK4 kinase genes cause pseudohypoaldosteronism type II, a familial disorder of renal potassium retention and hypertension (8), there has been great interest in understanding how these kinases normally control the balance between renal potassium excretion and sodium reabsorption. An emerging view holds the WNKs switch the aldosterone response of the kidney to be either kaliuretic or antinatriuretic, depending on whether aldosterone is induced by a change in potassium or by an alteration in the extracellular fluid volume. This likely occurs because the WNKs differently regulate the ROMK channel and the thiazide-sensitive sodium chloride cotransporter, NCC. Our discovery that ARH is a component of the WNK1 pathway, together with our recent observations with NCC (44), sheds light on the underlying mechanism.

Our ideas build on a rapidly evolving picture of a complex WNK signaling pathway and its involvement in the divergent regulation of NCC and ROMK. Work in model systems and genetically modified mouse models should leave little doubt that WNK4 has the capacity to inhibit NCC in the distal convoluted tubule (45–49). WNK4 has been reported to not affect ROMK remarkably in vivo (45, 46) even though it can have some inhibitory effects in heterologous expression systems (9, 12, 50). Instead, 2 WNK1 kinase isoforms (L-WNK1 and the kinase deficient form [KS-WNK1]) have opposing activities on ROMK and are differentially modulated

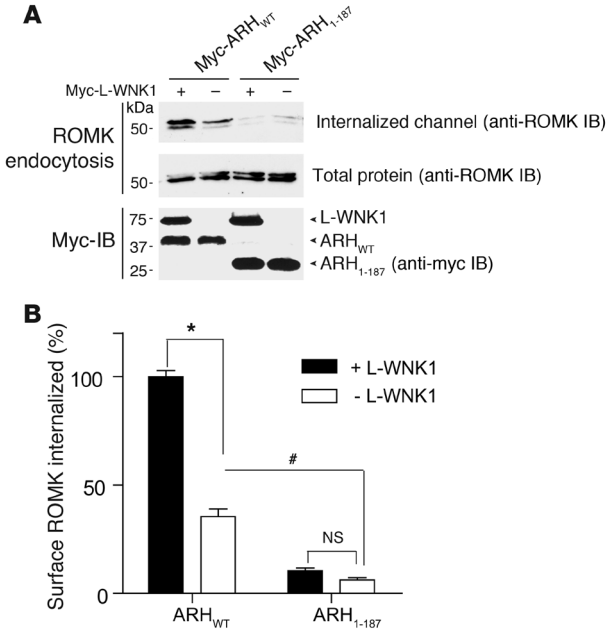


**Figure 8**
L-WNK1 stimulates ROMK endocytosis through an ARH-dependent mechanism. ROMK endocytosis was measured by biotinylation in COS-7 cells expressing either WT ARH (myc tagged, left column) or the dominant-negative ARH (myc-ARH$_{1–187}$) (right column) in the presence (+) or absence (-) of exogenous L-WNK1 (amino acids 1–491). (**A**) Representative experiment showing surface biotinylated ROMK channels that have become internalized after a 5-minute chase compared with the total surface pool (detected by immunoblot with anti-ROMK antibodies). (**B**) Quantification of ROMK endocytosis in cells cotransfected either WT ARH or ARH$_{1–187}$ and empty vector (white bars) or the active fragment of L-WNK1 (black bars) ($n = 3$). In the presence of WT ARH, L-WNK1 stimulated ROMK endocytosis. ($^*P < 0.001$). The response was completely suppressed by the dominant-negative ARH. Dominant-negative ARH also suppressed constitutive ROMK endocytosis ($^{\#}P < 0.05$).

in the kidney in response to changes in dietary potassium (10, 11), making it likely the WNK1 isoforms physiologically regulate ROMK to maintain potassium balance. Indeed, because the WNK1 isoforms regulate NCC oppositely of ROMK (via modulation of WNK4) (47, 51, 52), the WNK1 isoform switch can explain how the kidney manifests a kaliuretic response to an elevation in potassium and high aldosterone without altering sodium balance.

Our observations strongly suggest WNKs differentially regulate NCC and ROMK by modulating 2 distinct trafficking pathways. By directly measuring ROMK endocytosis for what we believe to be the first time, we found L-WNK1 stimulates internalization of the channel, verifying the prevailing view (9–12). More importantly, the discovery that ARH is necessary for WNK1-dependent regulation of ROMK establishes the identity of the relevant endocytotic mechanism and raises the possibility that ARH may be a substrate of L-WNK1, similar to the way the adaptor-associated kinase 1 (AAK1) regulates Numb function (53). Unlike ROMK, NCC does not contain NPXY type signals and, therefore, does not have the capacity to engage ARH. In fact, Subramanya et al. recently discovered that WNK4 does not stimulate NCC endocytosis (49). Instead, WNK4 acts on newly synthesized NCC in the secretory pathway to stimulate interaction with the AP-3 clathrin adaptor and divert the transporter into the lysosomal pathway. Collectively, these observations indicate that WNKs exert disparate effects on the 2 transport proteins, by modulating 2 distinct intracellular trafficking operations.

In summary, we have discovered that constitutive and WNK1-stimulated endocytosis in ROMK is controlled by ARH. What we believe to be a unique endocytotic signal in ROMK serves a recognition site for ARH interaction. Because ARH binds to clathrin and AP-2 through different structures than ROMK, ARH can effectively mark the channel for endocytosis to physiologically control ROMK surface density and, thereby, regulate potassium balance.

## Methods

*Molecular biology*. All studies were performed with the modified rat ROMK1, containing either an external HA epitope tag as described before (54) or an external Flag epitope. Site-directed mutagenesis was performed using a PCR-based strategy with PfuTubo DNA polymerase (QuikChange; Stratagene). The sequence of all modified cDNAs was confirmed by dye termination DNA sequencing (University of Maryland School of Medicine Biopolymer Core). cDNAs encoding ROMK1 cytoplasmic C-terminal regions (amino acids 349–391) were amplified by PCR from a full-length template (GenBank accession number NM017023) and cloned in-frame with GST in the vector pGEX-5x (Amersham Biosciences). The GST fusion of LRP C terminus was identical to that used in previous studies (23). All known human CLASPs that contain a PTB domain (ARH, DAB2, GULP, NUMB; provided by D. Strickland, University of Maryland School of Medicine) were subcloned in-frame to a His-tag in the pRSET vector (Invitrogen). Full-length ARH (GenBank accession number NP056442) and Numb (GenBank accession number NP001005745) were examined. Because of limited solubility of full-length Gulp and Dab2, smaller fragments of these proteins, containing their entire PTB domains, were studied (Dab2, GenBank accession number NP_001334, residues 1–220; Gulp, GenBank accession number NP_057399, residues 1–154). Studies with the L-WNK1 were performed using the active fragment (amino acids 1–491) as identified by He and coworkers (12). All constructs used for mammalian expression were subcloned into pcDNA 3.1+ (Invitrogen).

*Cell culture, transfection, lysis, and rat kidney homogenization*. COS-7 cells were cultured in a humidified atmosphere at 37°C in 5% $CO_2$ and grown in Dulbecco's modified Eagle's medium supplemented with 10% FBS, 100 U/ml penicillin, 100 μg/ml streptomycin, 10 mM HEPES, and 2 mM L-glutamine. Cells were transfected with 1–2 μg of plasmid using FuGENE 6 reagent (Roche Applied Science), according to the manufacturer's specifications. Cells were washed once in Ringer's solution, harvested in HEENG buffer (20 mM HEPES, pH 7.6, 25 mM NaCl, 1 mM EDTA, 1 mM EGTA, 10% glycerol), and then suspended in HEENG buffer containing 1% Triton X-100 and protease inhibitors. Cell lysates were incubated on ice for 45 minutes, and centrifuged to pellet insoluble material. Rat kidneys were placed in HEENG buffer containing a protease inhibitor cocktail and 1% Triton X-100 and homogenized using a Polytron (PT 10-35; Brinkman) tissue homogenizer. Protein concentrations were assessed by Bradford Assay (Bio-Rad).

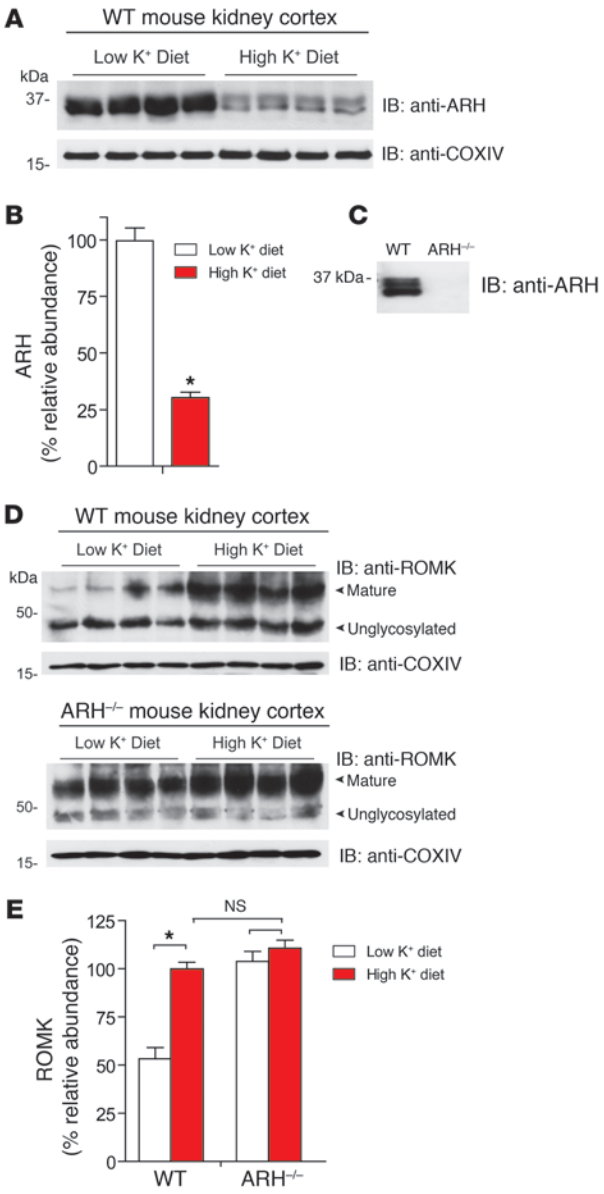


**Figure 9**
ARH is regulated by dietary potassium and controls ROMK in the kidney. (**A**) Representative anti-ARH Western blot of mouse kidney cortex isolated from WT mice fed either a low-potassium diet or a high-potassium diet. Each lane is from a different mouse. Cox IV was used as loading control. (**B**) Quantification of all experiments like those shown in **A**, indicating ARH protein abundance in the kidney ($n$ = 6/group; *$P$ < 0.001). (**C**) Representative anti-ARH Western blot in WT and ARH-knockout mice ($Arh^{-/-}$). (**D**) Representative anti-ROMK Western blot of mouse kidney cortex isolated from WT or ARH-knockout mice fed either a low-potassium diet or a high-potassium diet. Each lane is from a different mouse. Cox IV was used as loading control. (**E**) Quantification of total ROMK protein abundance (complex glycosylated plus unglycosylated) from all experiments like those shown in **D** ($n$ = 6/group; difference between high- and low-potassium diet, *$P$ < 0.001; the difference between either $Arh^{-/-}$ group is not significant, just as the difference between either $Arh^{-/-}$ group and WT mice fed the high-potassium diet is not significant.

*GST affinity chromatography*. GST-ROMK C-terminal fusion proteins and His-PTB adaptor proteins were produced in *Escherichia coli* (BL21; Invitrogen) and purified under nondenaturing conditions, using glutathione-Sepharose 4B affinity chromatography (Amersham Biosciences) or TALON Metal Affinity Resins (Clontech), as recommended by the manufacturer. Aliquots of Ni-NTA beads (Clontech) containing 2–5 μg of the recombinant His-tagged adaptor proteins were mixed with an equal quantity of each GST fusion protein in 300 μl of binding buffer (20 mM HEPES, 20 mM imidazole, 120 mM potassium acetate, and 0.1% Triton X-100, pH 7.5) and incubated for 45 minutes on a rotating platform at 4°C. Beads were collected by centrifugation (2,000 *g* for 5 minutes), unbound material was removed by aspiration, and beads were washed 3 times with 1 ml binding buffer. Proteins bound to beads were eluted in SDS sample buffer, resolved by SDS-PAGE, and then processed for Coomassie blue staining (Bio-Rad) or immunoblotting. For the latter, proteins were transferred electrophoretically to nitrocellulose membrane (Hybond; Amersham Biosciences) and probed with either a goat polyclonal anti-GST antibody (GE Healthcare) or a rabbit polyclonal anti-His (Santa Cruz Biotechnology Inc.) antibody, followed by HRP-conjugated secondary antibody (either mouse anti-goat IgG or goat-anti rabbit IgG at 1:5,000; Jackson ImmunoResearch Laboratories Inc.).

*Immunofluorescence and confocal microscopy*. COS-7 cells, grown on glass coverslips, were transfected as above. For the external HA-tagged N2.1/ROMKC antibody feeding studies, cells were studied 2 days after transfection when the majority of the channel was expressed on the cell surface. Cells were blocked (5% FBS in PBS, 30 minutes at room temperature), and surface channels were labeled with mouse, anti-HA antibody (Covance) at 4°C for 1 hour. After unbound antibody was removed (3 washes with PBS, 4°C), surface labeled channels were allowed to internalize for variable times at 37°C. Cells were then fixed (2% paraformaldehyde in PBS, 15 minutes at 4°C) and channels remaining at the surface were labeled with a saturating concentration of Alexa Fluor 488–conjugated goat anti-mouse secondary antibody. Internalized channels, labeled at the cell surface with HA antibody, were detected with Alexa Fluor 568–conjugated goat anti-mouse secondary antibody, following cell permeabilization (0.1% Triton X-100, 10 minutes at room temperature). After extensive washing with PBS buffer, the coverslips were mounted on glass slides with Vectashield (Vector Laboratories). The labeled cells were visualized under Zeiss 410 confocal microscopy using a ×63 oil immersion lens (numerical aperture, 1.40). Images were analyzed with the Volocity suite of imaging programs (Improvision Inc.).

*Immunolocalization of ARH and ROMK*. Sprague-Dawley rat kidneys were fixed in vivo by retrograde perfusion (2% freshly prepared paraformaldehyde in PBS), removed, sliced into large pieces, and then fixed additionally overnight and embedded in paraffin. Sections (3-μm thick) were picked up on coverslips by heat-induced target retrieval, and a citrate buffer (pH 8) was used to unmask epitopes. Sections were then washed and incubated overnight with primary antibodies to ARH raised in goat (Santa Cruz Biotechnology Inc.) or rabbit (Abcam) at a concentration of 5 μg/ml at 4°C, using methods and marker antibodies described previously (55). For ROMK colocalization, anti-chicken antibodies raised against the extreme C terminus of ROMK, as described and characterized before (56), were used. The antibody specifically detects appropriate molecular weight proteins in WT mice but not in ROMK null mice.

*Cell surface expression assay*. Surface expression of external HA epitope–tagged channels was detected and quantified by HA-antibody binding and chemiluminescence as described previously (54). Briefly, COS-7 cells were plated on 6-well tissue culture dishes and transfected with 1 μg of plasmid DNA using FuGENE6 reagent (Roche) at a 60% cell confluence. After 48 hours, cells were fixed (2% PFA in PBS), blocked (5% FBS in PBS buffer, 30 minutes), and incubated with mouse monoclonal anti-HA antibody (Covance). Cells were washed with PBS buffer (5 minutes, 3 times) and

incubated with goat anti-mouse IgG HRP-conjugated secondary antibody (Jackson ImmunoResearch Laboratories Inc.) for 30 minutes at room temperature. After unbound antibody was removed by extensive washing (PBS buffer 5 minutes, 3 times), cells were gently detached from the plate and suspended in 500 μl PBS buffer. Aliquots of the cell suspensions were combined with SuperSignal West Pico Chemiluminescent solution (Pierce), and chemiluminescence was measured using Sirius luminometer. Each suspension was measured in triplicate. Reported values represent the average of 3 separate transfections.

*Biotinylation internalization assay*. For studies of ROMK endocytosis by biotinylation, we incorporated a Flag tag epitope (DYKDDDDK) into the same external site as used for the HA-tag, as we have done before with Kir2.3 (57). The lysine residues in the external flag epitope tag provide free amino-group substrates for biotinylation. After transfection, cells were washed with ice-cold Ringer's solution (5 mM HEPES, 144 mM NaCl, 5 mM KCl, 1.2 mM $NaH_2PO_4$, 5.5 mM glucose, 1 mM $MgCl_2$, 1 mM $CaCl_2$, pH 7.4), and the surface proteins were biotinylated using EZ-link Sulfo-NHS-SS-Biotin (0.3 mg/ml, Pierce) in Ringer's solution for 1 hour at 4°C. Remaining biotin was quenched with 50 mM Tris, pH 7.5, in Ringer's solution for 20 minutes at 4°C. Cells were then placed at 37°C for variable times to allow internalization. The membrane-impermeant reducing agent MesNa (100 mM MesNa, 100 mM NaCl, 1 mM EDTA, 0.2% BSA, 50 mM Tris, pH 8.8) was added 3 times for 20 minutes at 4°C to cleave biotin linked to the cell surface. Cells were then washed 3 times with Ringer's solution and lysed. Biotinylated proteins were recovered by adding the cell lysate (100 μg) to neutravidin beads (Pierce) in PBS buffer containing 0.1% SDS and rotating overnight at 4°C. Beads were washed 3 times with PBS buffer plus 0.1% SDS, and biotinylated protein was eluted from the beads with 6x SDS sample buffer (45 minutes at room temperature). Proteins were resolved by SDS-PAGE and subjected to Western blot analysis with anti-ROMK antibodies. Anti-actin antibodies were used as a control to check for spurious intracellular biotinylation.

*Biotinylation cell surface assay*. Channels at the cell surface were biotinylated as above, and remaining biotin was quenched with 50 mM Tris, pH 7.5, in Ringer's solution for 20 minutes at 4°C. Cells were then washed 3 times with Ringer's solution and lysed, and 100 μg of total protein was added to neutravidin beads in PBS buffer containing 0.1% SDS and rotated overnight at 4°C. Beads were washed 3 times with PBS buffer plus 0.1% SDS, and biotinylated protein was eluted from the beads with 6x SDS sample buffer (45 minutes at room temperature). Proteins were resolved by SDS-PAGE and subject to Western blot analysis as above.

*Immunoprecipitation and Western blot analysis*. Solubilized cell lysates or tissue homogenates were incubated overnight with the appropriate antibodies and Protein G Plus Protein A beads (Calbiochem). Beads were washed 3 times with PBS buffer and then eluted for 30 minutes at room temperature with SDS-sample buffer. Eluates were separated by SDS-PAGE, transferred to nitrocellulose membranes, and blocked in Tris-buffered saline with 0.1% Tween 20 (TBS-T) containing 5% non-fat dry milk (NFDM) for 1 hour at room temperature. Membranes were then incubated in 5% NFDM containing primary antibody (overnight at 4°C), washed in TBS-T, incubated in 5% NFDM containing HRP-conjugated secondary antibody, and then washed for 10 minutes (3 times) in TBS-T. Bound antibodies were then revealed using enhanced chemiluminescence reagent (Pierce) and fluorography. Densitometric measurements were made using Quantity One.

*siRNA knockdown*. Knockdown experiments in COS-7 cells were performed as described by Maurer et al. (19) with several minor changes. COS-7 cells (50% confluent) were plated in 12-well plates. Twenty-four hours later, cells were transfected with of a pool of 4 siRNA oligonucleotides (50 nmol) specific for ARH (Dharmacon) or a nontargeting siRNA pool as a negative control (Dharmacon) using Oligofectamine (Invitrogen). Oligonucleotide transfection was repeated twice, on day 1 and day 3. On day 4, cells were used to study ROMK endocytosis.

*ARH null mouse experiments*. Age-matched (6–8 weeks), weight-matched (20–25 grams), and sex-matched (male) WT litter mates were compared with male mice documented to be homozygous for knockout of the *ARH* gene ($Arh^{-/-}$), provided by H. Hobbs (University of Texas Southwestern Medical Center). All protocols used in the studies described were approved by the Institutional Animal Care and Use Committee at the University of Maryland Medical School. As previously described (41), $Arh^{-/-}$ mice were created by replacement of exon 4, encoding the PTB domain, with a neomycin selection cassette that was flanked by both loxP and FRT sites. $Arh^{-/-}$ mice are fertile, normal in size, and do not display any gross physical or behavioral abnormalities. Mice were maintained on standard chow and water ad libitum. Before the experimental procedure, animals were placed on a control diet (1% potassium, TD.88238; Harlan Teklad), which is precisely matched for equal caloric content of the experimental diets. After 3 days, mice were assigned to 1 of 2 treatment groups: (a) high-potassium diet for 4 days (10% potassium diet TD.09075; Harlan Teklad); (b) potassium-deficient diet for 4 days (0% potassium diet TD.09075; Harlan Teklad). After the treatment period, mice were anesthetized with isoflurane, and the kidneys were rapidly removed, and the renal cortex was dissected and flash frozen in liquid nitrogen. Samples were placed in ice-cold HEENG buffer solution (20 mM HEPES, pH 7.6, 25 mM NaCl, 1 mM EDTA, 1 mM EGTA, 10% glycerol, pH 7.6, containing protease inhibitor cocktail [P8340; Sigma-Aldrich], 1% Triton X-100 and 0.5% SDS), homogenized in ice-cold isolation solution using a Polytron tissue homogenizer, and then rotated at 4°C for 1 hour. The samples were centrifuged at approximately 15,000 *g* for 10 minutes at 4°C to pellet insoluble material. Protein concentration was measured using a bicinchoninic acid protein assay reagent kit (Pierce). Equal amounts of kidney protein were suspended in Laemmli buffer (room temperature for 45 minutes) and loaded on 10% SDS-PAGE gels for Western blot analysis as described above, with anti-rabbit antibodies raised against the extreme C terminus of ROMK as described and characterized before (56), or ARH (purchased from Abcam or provided by H. Hobbs; refs. 39, 41), or a loading control (anti-COXIV; Abcam). The ROMK antibody specifically detects appropriate molecular weight proteins in WT mice but not in ROMK null mice. Likewise, both ARH antibodies detect predicted sized species in WT mice but not in ARH null mice.

*Statistics*. Data are presented as mean ± SEM. Statistical analysis was performed using GraphPad PRISM version 5. Statistical significance was determined by 2-tailed Student's *t* test when comparing 2 groups and by 1-way randomized ANOVA, followed by Bonferroni's post-hoc test, when comparing multiple groups or Dunnett's post-hoc test when test groups were compared with the control. *P* values of less than 0.05 were considered statistically significant.

## Acknowledgments

This was study was supported by funds from the NIDDK, NIH (grants DK54281 and DK63049 to P.A. Welling; grant DK-32839 to J.B. Wade). We are grateful to Dudley Strickland and Helen Hobbs for providing valuable reagents and to Stephanie Blankenship for her expert technical help with the mice.

Received for publication November 3, 2008, and accepted in revised form August 26, 2009.

Address correspondence to: Paul A. Welling, Department of Physiology, University of Maryland Medical School, 655 W. Baltimore, Baltimore, Maryland 21201, USA. Phone: (410) 706-3851; Fax: (410) 706-8341; E-mail: pwelling@umaryland.edu.

1. Ho, K., et al. 1993. Cloning and expression of an inwardly rectifying ATP-regulated potassium channel. *Nature.* **362**:31–38.
2. Hebert, S.C., Desir, G., Giebisch, G., and Wang, W. 2005. Molecular diversity and regulation of renal potassium channels. *Physiol. Rev.* **85**:319–371.
3. Mennitt, P.A., Wade, J.B., Ecelbarger, C.A., Palmer, L.G., and Frindt, G. 1997. Localization of ROMK channels in the rat kidney. *J. Am. Soc. Nephrol.* **8**:1823–1830.
4. Lee, W.S., and Hebert, S.C. 1995. ROMK inwardly rectifying ATP-sensitive K+ channel. I. Expression in rat distal nephron segments. *Am. J. Physiol.* **268**:F1124–F1131.
5. Kohda, Y., et al. 1998. Localization of the ROMK potassium channel to the apical membrane of distal nephron in rat kidney. *Kidney Int.* **54**:1214–1223.
6. Palmer, L.G., and Frindt, G. 2000. Aldosterone and potassium secretion by the cortical collecting duct. *Kidney Int.* **57**:1324–1328.
7. Zeng, W.Z., et al. 2002. Evidence for endocytosis of ROMK potassium channel via clathrin-coated vesicles. *Am. J. Physiol. Renal Physiol.* **283**:F630–F669.
8. Wilson, F.H., et al. 2001. Human hypertension caused by mutations in WNK kinases. *Science.* **293**:1107–1112.
9. Kahle, K.T., et al. 2003. WNK4 regulates the balance between renal NaCl reabsorption and K+ secretion. *Nat. Genet.* **35**:372–376.
10. Lazrak, A., Liu, Z., and Huang, C.L. 2006. Antagonistic regulation of ROMK by long and kidney-specific WNK1 isoforms. *Proc. Natl. Acad. Sci. U. S. A.* **103**:1615–1620.
11. Wade, J.B., et al. 2006. WNK1 kinase isoform switch regulates renal potassium excretion. *Proc. Natl. Acad. Sci. U. S. A.* **103**:8558–8563.
12. He, G., Wang, H.R., Huang, S.K., and Huang, C.L. 2007. Intersectin links WNK kinases to endocytosis of ROMK1. *J. Clin. Invest.* **117**:1078–1087.
13. Chen, W.J., Goldstein, J.L., and Brown, M.S. 1990. NPXY, a sequence often found in cytoplasmic tails, is required for coated pit-mediated internalization of the low density lipoprotein receptor. *J. Biol. Chem.* **265**:3116–3123.
14. Davis, C.G., van Driel, I.R., Russell, D.W., Brown, M.S., and Goldstein, J.L. 1987. The low density lipoprotein receptor. Identification of amino acids in cytoplasmic domain required for rapid endocytosis. *J. Biol. Chem.* **262**:4075–4082.
15. Bonifacino, J.S., and Traub, L.M. 2003. Signals for sorting of transmembrane proteins to endosomes and lysosomes. *Annu. Rev. Biochem.* **72**:395–447.
16. Traub, L.M., and Lukacs, G.L. 2007. Decoding ubiquitin sorting signals for clathrin-dependent endocytosis by CLASPs. *J. Cell Sci.* **120**:543–553.
17. Uhlik, M.T., et al. 2005. Structural and evolutionary division of phosphotyrosine binding (PTB) domains. *J. Mol. Biol.* **345**:1–20.
18. Keyel, P.A., et al. 2006. A single common portal for clathrin-mediated endocytosis of distinct cargo governed by cargo-selective adaptors. *Mol. Biol. Cell.* **17**:4300–4317.
19. Maurer, M.E., and Cooper, J.A. 2006. The adaptor protein Dab2 sorts LDL receptors into coated pits independently of AP-2 and ARH. *J. Cell Sci.* **119**:4235–4246.
20. Morris, S.M., Tallquist, M.D., Rock, C.O., and Cooper, J.A. 2002. Dual roles for the Dab2 adaptor protein in embryonic development and kidney transport. *EMBO J.* **21**:1555–1564.
21. Mishra, S.K., et al. 2002. Disabled-2 exhibits the properties of a cargo-selective endocytic clathrin adaptor. *EMBO J.* **21**:4915–4926.
22. Santolini, E., et al. 2000. Numb is an endocytic protein. *J. Cell Biol.* **151**:1345–1352.
23. Ranganathan, S., et al. 2004. Serine and threonine phosphorylation of the low density lipoprotein receptor-related protein by protein kinase Calpha regulates endocytosis and association with adaptor molecules. *J. Biol. Chem.* **279**:40536–40544.
24. Mishra, S.K., Watkins, S.C., and Traub, L.M. 2002. The autosomal recessive hypercholesterolemia (ARH) protein interfaces directly with the clathrin-coat machinery. *Proc. Natl. Acad. Sci. U. S. A.* **99**:16099–16104.
25. He, G., et al. 2002. ARH is a modular adaptor protein that interacts with the LDL receptor, clathrin, and AP-2. *J. Biol. Chem.* **277**:44044–44049.
26. Garcia, C.K., et al. 2001. Autosomal recessive hypercholesterolemia caused by mutations in a putative LDL receptor adaptor protein. *Science.* **292**:1394–1398.
27. Nagai, M., Meerloo, T., Takeda, T., and Farquhar, M.G. 2003. The adaptor protein ARH escorts megalin to and through endosomes. *Mol. Biol. Cell.* **14**:4984–4996.
28. Paccaud, J.P., et al. 1993. Clathrin-coated pit-mediated receptor internalization. Role of internalization signals and receptor mobility. *J. Biol. Chem.* **268**:23191–23196.
29. Mishra, S.K., et al. 2005. Functional dissection of an AP-2 beta2 appendage-binding sequence within the autosomal recessive hypercholesterolemia protein. *J. Biol. Chem.* **280**:19270–19280.
30. Liu, Z., Wang, H.R., and Huang, C.L. 2009. Regulation of ROMK channel and K+ homeostasis by kidney-specific WNK1 kinase. *J. Biol. Chem.* **284**:12198–12206.
31. Frindt, G., Shah, A., Edvinsson, J., and Palmer, L.G. 2009. Dietary K regulates ROMK channels in connecting tubule and cortical collecting duct of rat kidney. *Am. J. Physiol. Renal Physiol.* **296**:F347–F354.
32. Wang, W., Schwab, A., and Giebisch, G. 1990. Regulation of small-conductance K channel in apical membrane of rat cortical collecting tubule. *Am. J. Physiol.* **259**:F494–F502.
33. Palmer, L.G., Antonian, L., and Frindt, G. 1994. Regulation of apical K and Na channels and Na/K pumps in rat cortical collecting tubule by dietary K. *J. Gen. Physiol.* **104**:693–710.
34. Chu, P.Y., Quigley, R., Babich, V., and Huang, C.L. 2003. Dietary potassium restriction stimulates endocytosis of ROMK channel in rat cortical collecting duct. *Am. J. Physiol. Renal Physiol.* **285**:F1179–F1187.
35. Davis, C.G., et al. 1986. The J.D. mutation in familial hypercholesterolemia: amino acid substitution in cytoplasmic domain impedes internalization of LDL receptors. *Cell.* **45**:15–24.
36. Rabb, H., Michishita, M., Sharma, C.P., Brown, D., and Arnaout, M.A. 1993. Cytoplasmic tails of human complement receptor type 3 (CR3, CD11b/CD18) regulate ligand avidity and the internalization of occupied receptors. *J. Immunol.* **151**:990–1002.
37. Li, S.C., et al. 1998. Structure of a Numb PTB domain-peptide complex suggests a basis for diverse binding specificity. *Nat. Struct. Biol.* **5**:1075–1083.
38. Jones, C., et al. 2007. Disruption of LDL but not VLDL clearance in autosomal recessive hypercholesterolemia. *J. Clin. Invest.* **117**:165–174.
39. Garuti, R., et al. 2005. The modular adaptor protein autosomal recessive hypercholesterolemia (ARH) promotes low density lipoprotein receptor clustering into clathrin-coated pits. *J. Biol. Chem.* **280**:40996–41004.
40. Michaely, P., Li, W.P., Anderson, R.G., Cohen, J.C., and Hobbs, H.H. 2004. The modular adaptor protein ARH is required for low density lipoprotein (LDL) binding and internalization but not for LDL receptor clustering in coated pits. *J. Biol. Chem.* **279**:34023–34031.
41. Jones, C., et al. 2003. Normal sorting but defective endocytosis of the low density lipoprotein receptor in mice with autosomal recessive hypercholesterolemia. *J. Biol. Chem.* **278**:29024–29030.
42. Saito, A., Pietromonaco, S., Loo, A.K., and Farquhar, M.G. 1994. Complete cloning and sequencing of rat gp330/"megalin," a distinctive member of the low density lipoprotein receptor gene family. *Proc. Natl. Acad. Sci. U. S. A.* **91**:9725–9729.
43. Leheste, J.R., et al. 1999. Megalin knockout mice as an animal model of low molecular weight proteinuria. *Am. J. Pathol.* **155**:1361–1370.
44. Subramanya, A.R., Liu, J., Ellison, D.H., Wade, J.B., and Welling, P.A. 2009. WNK4 Diverts the Thiazide-sensitive NaCl Cotransporter to the Lysosome and Stimulates AP-3 Interaction. *J. Biol. Chem.* **284**:18471–18480.
45. Lalioti, M.D., et al. 2006. Wnk4 controls blood pressure and potassium homeostasis via regulation of mass and activity of the distal convoluted tubule. *Nat. Genet.* **38**:1124–1132.
46. Yang, S.S., et al. 2007. Molecular pathogenesis of pseudohypoaldosteronism type II: generation and analysis of a Wnk4(D561A/+) knockin mouse model. *Cell Metab.* **5**:331–344.
47. Yang, C.L., Angell, J., Mitchell, R., and Ellison, D.H. 2003. WNK kinases regulate thiazide-sensitive Na-Cl cotransport. *J. Clin. Invest.* **111**:1039–1045.
48. Wilson, F.H., et al. 2003. Molecular pathogenesis of inherited hypertension with hyperkalemia: the Na-Cl cotransporter is inhibited by wild-type but not mutant WNK4. *Proc. Natl. Acad. Sci. U. S. A.* **100**:680–684.
49. Subramanya, A.R., Liu, J., Ellison, D.H., Wade, J.B., and Welling, P.A. 2009. WNK4 diverts the thiazide-sensitive NaCl cotransporter to the lysosome and stimulates AP-3 interaction. *J. Biol. Chem.* **284**:18471–18480.
50. Ring, A.M., et al. 2007. An SGK1 site in WNK4 regulates Na+ channel and K+ channel activity and has implications for aldosterone signaling and K+ homeostasis. *Proc. Natl. Acad. Sci. U. S. A.* **104**:4025–4029.
51. Yang, C.L., Zhu, X., Wang, Z., Subramanya, A.R., and Ellison, D.H. 2005. Mechanisms of WNK1 and WNK4 interaction in the regulation of thiazide-sensitive NaCl cotransport. *J. Clin. Invest.* **115**:1379–1387.
52. Subramanya, A.R., Yang, C.L., Zhu, X., and Ellison, D.H. 2006. Dominant-negative regulation of WNK1 by its kidney-specific kinase-defective isoform. *Am. J. Physiol. Renal Physiol.* **290**:F619–F624.
53. Sorensen, E.B., and Conner, S.D. 2008. AAK1 Regulates numb function at an early step in clathrin-mediated endocytosis. *Traffic.* **9**:1791–1800.
54. Yoo, D., et al. 2003. Cell surface expression of the ROMK (Kir 1.1) channel is regulated by the aldosterone-induced kinase, SGK-1, and protein kinase A. *J. Biol. Chem.* **278**:23066–23075.
55. Coleman, R.A., Liu, J., and Wade, J.B. 2006. Use of anti-fluorophore antibody to achieve high-sensitivity immunolocalizations of transporters and ion channels. *J. Histochem. Cytochem.* **54**:817–827.
56. Ecelbarger, C.A., et al. 2001. Regulation of potassium channel Kir 1.1 (ROMK) abundance in the thick ascending limb of Henle's loop. *J. Am. Soc. Nephrol.* **12**:10–18.
57. Mason, A.K., Jacobs, B.E., and Welling, P.A. 2008. AP-2-dependent internalization of potassium channel Kir2.3 is driven by a novel di-hydrophobic signal. *J. Biol. Chem.* **283**:5973–5984.